Fusion Engineering and Design 126 (2018) 67–72

Contents lists available at ScienceDirect

Fusion Engineering and Design

journal homepage: www.elsevier.com/locate/fusengdes

Design and RF test of a prototype traveling wave antenna for helicon current drive in KSTAR

H.H. Wi*, S.J. Wang, H.J. Kim, J.G. Kwak

National Fusion Research Institute, 169-148 Gwahak-ro, Yuseong-gu, Daejeon 34133, South Korea

ARTICLE INFO

Keywords:
Traveling wave antenna
Helicon current drive
Fast wave
RF wave heating
KSTAR
Combline antenna

ABSTRACT

Non-inductive current drive by fast wave at very high ion cyclotron harmonics, known as 'helicons' has the potential for high off-axis current drive efficiency compared with the other known non-inductive current drive techniques. However, non-inductive current drive by helicon wave has not been validated experimentally. To validate its anticipated performance experimentally, an antenna design is one of the most important issues. A Traveling wave antenna has particularly valuable features for launching the fast wave such as load resiliency, narrow $n_{||}$ spectrum, and simple RF circuits without additional-external matching systems. Low power level helicon wave coupling experiments has been conducted successfully using a mock-up TWA in KSTAR. In the next step, in order to investigate a high power performance, a new prototype TWA based on the mock-up TWA has been designed, fabricated and measured for a medium power (100–300 kW) RF system. The prototype TWA having a Faraday shield was made of copper and consists of 10 current straps with 5 inch coaxial feeding lines as input and output ports. The detailed design parameters and electromagnetic characteristics of prototype TWA are discussed.

1. Introduction

An important goal of the KSTAR tokamak is to develop advanced scenarios ($\beta_N > 3$) with non-inductive current drive for steady-state operation [1]. Several predictions show that non-inductive current drive by absorption of fast waves at very high ion cyclotron harmonics, known as helicons has the potential for high current drive efficiency compared to other known non-inductive current drive methods [2–4]. However, non-inductive current drive by helicon wave has not been validated experimentally. Therefore, the basis of physics and engineering issue of helicon current drive has been investigated in KSTAR tokamak. The primary challenge is to design an antenna that can couple an RF wave to the plasma while maintain the good impedance matching during abrupt changes of plasma characteristics such as L/H-mode transitions, and edge localized mode activity. The antenna should also impose the desired value of parallel refractive index ($n_{||}$), and the electric field polarization at the launcher must be controlled so as to excite primarily the fast wave. The traveling wave antenna (TWA) is an attractive option because of its insensitivity to the variation of loading resistance without additional-external matching circuit and it already showed good performances in the other tokamak experiments [5–7].

The first step of the helicon current drive experiment was to construct a low power (mW) mock-up combline-type TWA, to install it into the KSTAR tokamak, and to measure the coupling and impedance matching properties in an L/H-mode plasma, in order to resolve an engineering and physics issue for high power helicon current drive. The coupling measurement was performed using a two port vector network analyzer (VNA: Agilent E5071C), which was connected to the input and output ports of mock-up TWA installed in KSTAR vacuum vessel. Various experiments have been conducted on a variety of plasma conditions to measure the variation of impedance matching, coupling, and change of dominant $n_{||}$ [8]. To distinguish the slow and fast wave couplings, the magnetic pitch angle was scanned during a discharge for both L/H-mode plasmas. The experimental and analytical results show that the fast wave was dominant in fairly high coupling, and load resiliency can be obtained by using the TWA concept [8].

In the next step, the most important aspects that remained to be addressed, both theoretically and experimentally, have to do with the wave propagation and absorption, stray heating channels such as scrape-off layer heating, and the non-linear aspects of wave such as parametric decay instability, in addition to the current driving capability [9,10]. In order to investigate these issues in helicon current drive, a medium power, 100–300 kW, RF system has been developed. The detailed configuration and characteristics of RF system including RF source, transmission line layout, and RF vacuum window will be published elsewhere.

* Corresponding author.
E-mail address: hhwi@nfri.re.kr (H.H. Wi).

https://doi.org/10.1016/j.fusengdes.2017.11.016
Received 7 March 2017; Received in revised form 20 November 2017; Accepted 20 November 2017
Available online 01 December 2017

In this paper, we focused on the design and analysis of prototype TWA for high power helicon current drive, and discuss its detailed electromagnetic characteristics including the scattering parameters and $n_{||}$ spectrum based on the simulation and measurements. All electromagnetic simulations in this work has been done with commercial software package, CST MWS [11].

2. Design and simulation results of TWA

2.1. Basic properties of TWA

A TWA is a class of antenna that uses a traveling wave on a guiding structure with continuous or periodic radiating structure. A simple example is a slotted waveguide antenna, where the waveguide is perturbed with periodic slots in the structure at a certain position. The reasonable design goal of TWA is to have most of the power in the waveguide radiated from the structure when the wave propagates through the entire structure while maintaining good impedance matching. If the length of TWA is infinitely long, it radiates all RF wave, but in the most of realistic TWA, a matched load will be connected at the end of antenna in order to absorb the remainder of the incident power.

The TWA can be represented by a simplified equivalent circuit model as shown in Fig. 1, which consists of infinite radiating structure elements in the longitudinal direction. Where R represents the sum of Ohmic loss and resistive loading, M is the mutual reactance between neighboring radiating structure elements. The incident power is transmitted to the adjacent radiating structure elements by mutual reactance, and the rest of power is radiated. If the number of radiating structure elements are infinite, then all the incident energy is radiated while the incident power is transferred to the next radiating element in sequence. If the resistive term is much smaller than the mutual reactance, then the input impedance of TWA can be approximately expressed as an Eq. (1) [12].

$$Z_{in} = \omega M\left[1 - \frac{1}{8}\left(\frac{R}{\omega M}\right)^2 + \ldots\right] \tag{1}$$

Eq. (1) means that input impedance of the TWA is nearly independent of the resistive loading, and this is the fundamental principle that makes the TWA is load resilient.

Among the various TWA types, a combline antenna was chosen for testing helicon current drive experiment in KSTAR. A combline antenna consists of several poloidal current straps placed in toroidal direction with only two external connections, the input and output port, and it was equivalent to an RF band pass filter if the radiation was neglected [13]. The current straps are inductively coupled and generate a slow wave structure along the toroidal direction inside the antenna box. This is a very valuable feature which can launch the desired $n_{||}$ spectrum.

2.2. Mock-up TWA

The mock-up TWA for 500 MHz was designed based on the combline filter design theory. The mock-up TWA was made of stainless steel and consists of 7 current straps with N-type input and output connectors as shown in Fig. 2. The dimensions of the mock-up TWA were 600 mm, 200 mm, and 50 mm in the toroidal, poloidal, and radial directions, respectively. The spacing (D) between current straps was 68 mm. The dimensions of the current straps are 20 mm, 130 mm, and 10 mm in the toroidal, poloidal, and radial direction respectively. The electrical length of current strap (L1) and gap between end of current strap and ground box (L2) represent the inductance and capacitance, respectively, which were important design parameters in combline antenna design.

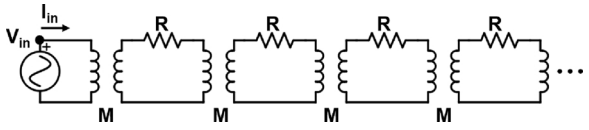

Fig. 1. Simplfied equivalent circuit model of semi-infinite TWA.

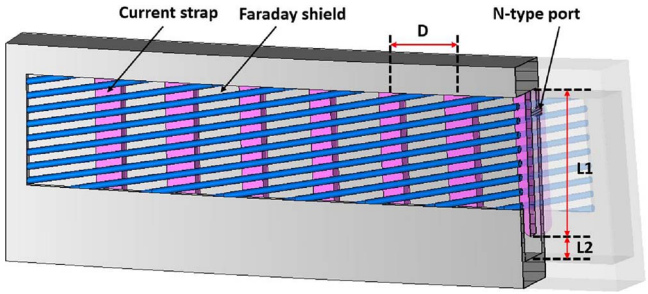

Fig. 2. 3D model of mock-up TWA.

The feeding structure of the antenna can be simplified to a monopole antenna with capacitance by L2, where the resonant frequency is determined by the combination of L1 and L2. The impedance bandwidth of combline antenna is mainly determined by L1, and the optimum electrical length(θ) of L1 is approximately 53° to achieve the maximum impedance bandwidth [14,15].

$$\mathrm{BW} = \mathrm{k}\frac{\theta\tan(\theta)}{\tan(\theta) + \theta(1 + tan^2(\theta))} \tag{2}$$

Eq. (2) shows the impedance bandwidth dependence on the electrical length of current strap, where K was a constant that depends on the current strap geometry. In order to obtain the maximum impedance bandwidth, the required capacitance was also increased, which causes an increase in the electric field strength at the end of current straps. To reduce electric field strength, the shape of the end of current straps was designed as a round shape as shown in Fig. 2. Although mock-up TWA was intended for low power test, electric field strength has been considered for the high power prototype TWA. By considering both the impedance bandwidth and electric field strength, the electrical length of current straps was determined to be approximately 78°. The Faraday shield was used to launch the fast wave, and it was tilted by 10° considering alignment with the fixed magnetic field for targeted discharge in KSTAR [16].

The power spectrum was calculated from the electric field along a line parallel to the Faraday shield above 10 mm as shown in Fig. 3. The peak $n_{||}$ of mock-up TWA was 3 at 500 MHz, which was considered to be the optimal value for helicon current drive in KSTAR [17].

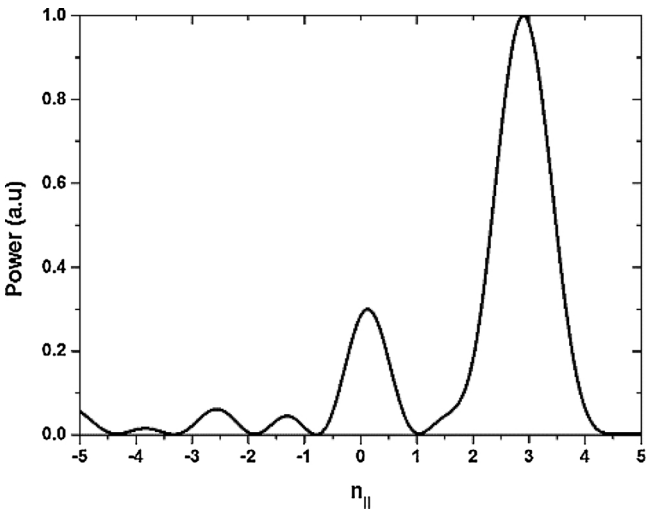

Fig. 3. Calculated power spectrum of the mock-up TWA at 500 MHz.

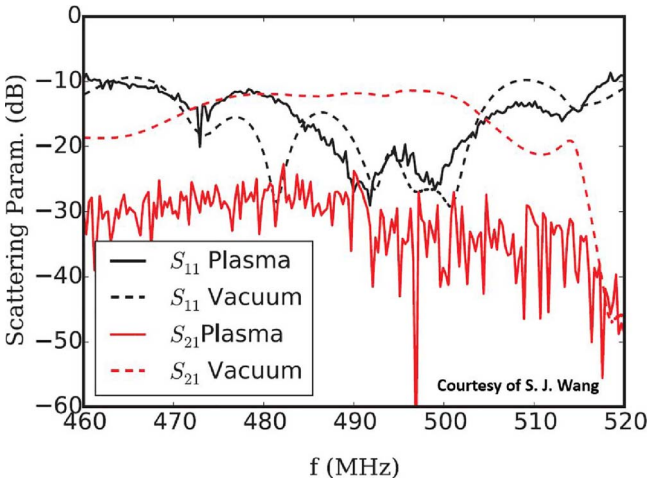

Fig. 4. Measured result of mock-up TWA, which depends on the vacuum or plasma loading.

Fig. 4 shows scattering parameters, $S_{11} = V_r/V_f$, and $S_{21} = V_t/V_f$, where V_f, V_r, and V_t are forward, reflected and transmitted voltages, respectively, of mock-up TWA with vacuum or plasma loading [8]. Approximately −10 dB offset was caused by the un-calibrated lossy cables located in the KSTAR vacuum vessel connecting N-type connectors at the TWA and the RF vacuum feedthrough. When we measured the coupling using VNA, the input power and sweep time are 10dBm, 20 ms respectively. The operating frequency of mock-up TWA was 500 MHz for coupling experiments, which was approximately 10 MHz above the center frequency of the passband. Although the center frequency of the mockup antenna was 490 MHz, the calculated peak $n_{||}$ value was 2.8. The peak $n_{||}$ value calculated at 500 MHz was 3, so the experiment was conducted at 500 MHz. In the vacuum loading case, the scattering parameters represent typical band pass filter characteristics, but in the plasma loading case, the transmission coefficient S_{21} was significantly reduced while maintaining similar reflection coefficient S_{11} with vacuum loading. In the case of plasma loading conditions, the plasma change makes a variation of S_{21}.

2.3. Design of the prototype TWA

The prototype TWA was designed through considering the coupling results of mock-up antenna and power handling capabilities. The previous experimental results using the mock-up TWA had shown that the $n_{||}$ was distorted when it was operated with too high a coupling around 70–100% [8]. The fundamental solution is to increase the total number of straps while reducing the coupled energy per unit strap. However, it was difficult to increase the number of current straps sufficiently because the allocated installation area was limited. Therefore, when designing the prototype TWA, the distance between the straps was reduced from 68 mm to 50 mm so that 10 straps can be installed in the same space. Also, the center frequency of the pass band was designed to be corrected to 500 MHz, and the bandwidth was also increased by adjusting the length of the currrent straps. In order to deliver more higher power, the N-type feed line was re-designed with a 5-inch coaxial feed line. The Faraday shield structure was designed by adding a support structure between the straps in order to support it more robustly.

2.3.1. Configuration of the prototype TWA

The prototype TWA was made of copper to reduce the Ohmic loss and consists of 10 current straps with 5 inch coaxial lines as input and output ports as shown in Fig. 4. The dimensions of the prototype TWA were almost the same as the mock-up TWA. The dimensions of the current straps are 28 mm, 122 mm, and 14 mm in the toroidal, poloidal, and radial directions respectively. The electrical length of current straps (~72°) was slightly reduced to adjust the center frequency of prototype to 500 MHz. The spacing between current straps was adjusted to 50 mm by considering the $n_{||} = 3$ at 500 MHz. To avoid the slow wave excitation, magnetic field aligned Faraday shield was adopted and the slanting angle was slightly reduced to 8° for new reference plasma equilibrium parameters. To enhance the power handling capabilities compared with the low power mock-up TWA, 5 inch input and output coaxial feeders were adapted. Coaxial inner conductor supports with 10 mm thick alumina ceramic ($\varepsilon_r = 9.5$, $tan\delta < 5 \times 10^{-4}$), were inserted into the antenna side and transmission line side respectively as shown in Fig. 5.

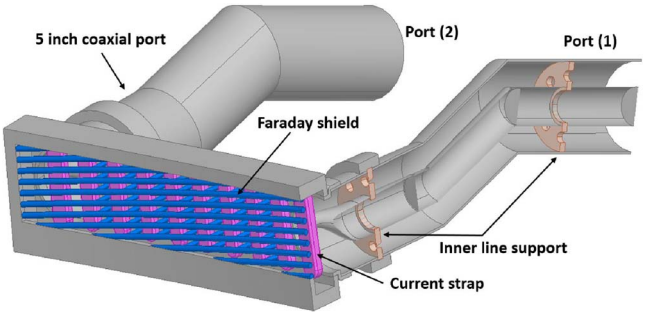

Fig. 5. 3D model of prototype TWA.

2.3.2. Simulated results of prototype TWA with vacuum loading

In order to simulated the electromagnetic performance of the antenna, an additional air gap of 200 mm was set in all directions except for the feeding part plane, and the outermost plane was set to the PML (Perfectly Matched Layer) condition. The outermost plane of +X direction, which is the plane of the feeding direction of the antenna, is set to PEC (Perfect Electric Conductor) layer as shown in Fig. 6.

Fig. 7 shows the simulation results of the scattering parameters of the prototype TWA with vacuum loading case and it shows typical band pass filter characteristics.

The impedance bandwidth of prototype TWA was approximately 30 MHz ($S_{11} < -20$ dB), which was increased compared to the mock-up TWA due to the decrease of the electrical length of current straps. In the pass band, the S_{21} was almost 0 dB. The Ohmic loss was ignored in the simulation.

Fig. 8 shows the calculated power spectra of mock-up and the prototype TWAs. The peak $n_{||}$ value of the prototype TWA is 3, which is as the mock-up TWA one, and the power spectrum of prototype TWA is slightly narrower than that of mock-up TWA because of the larger number of current straps.

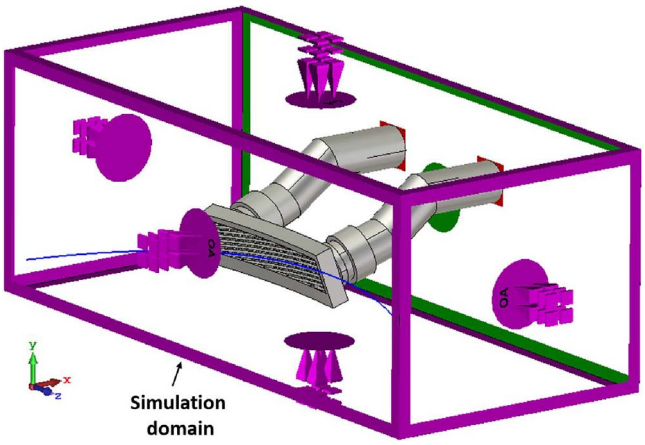

Fig. 6. Boundary condition for antenna simulation.

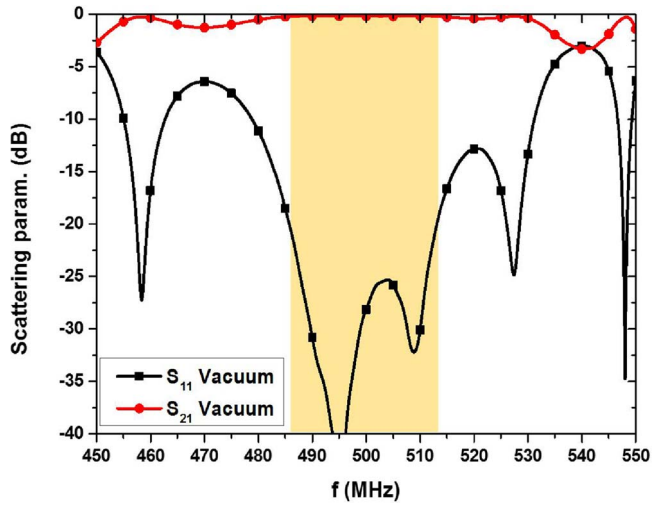

Fig. 7. Simulated scattering parameters of prototype TWA.

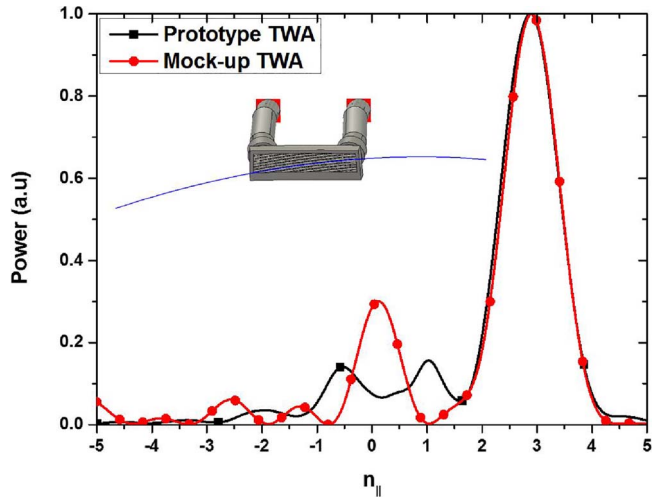

Fig. 8. Calculated power spectrums of the mock-up and prototype TWAs at 500 MHz.

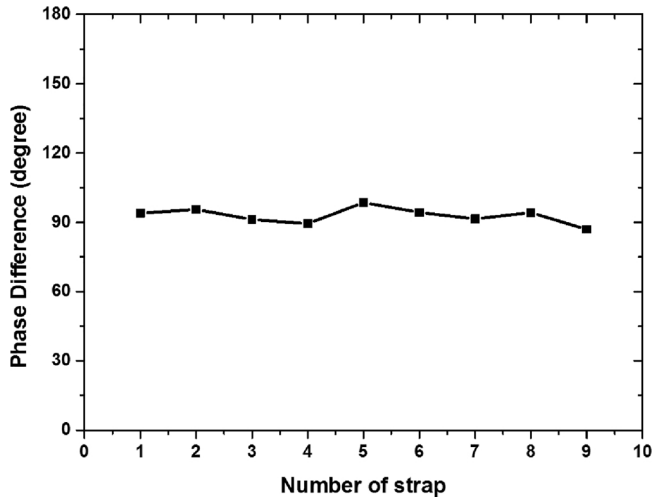

Fig. 9. Phase difference between the neighboring straps at 500 MHz.

According to the combline filter design theory [18], the phase difference between the neighboring current straps in the center frequency of pass band is 90°. The result of calculating the phase difference with neighboring straps is in good agreement with the theoretical result as shown in Fig. 9. The $n_{||}$ may be defined as [19],

$$n_{||} \equiv c\frac{k_{||}}{\omega} \approx \frac{\Delta\phi}{d} \times \frac{c}{2\pi f}, \tag{2}$$

where c is the speed of light, $k_{||}$ is the toroidal wavenumber, Δϕ and d are the phase difference and spacing between the neighboring current straps, respectively. When d = 50 mm, Δϕ = 90°, and f = 500 MHz, it was calculated to be $n_{||}$ = 3 and this value was in good agreement with calculated peak spectrum as shown in Fig. 8.

2.3.3. Simulated results of prototype TWA with simplified plasma loading

The 3D full-wave analysis considering both the magnetized-hot plasma and arbitrary antenna structure is not easily supported by the commercial EM simulator such as CST MWS [11] and ANSYS HFSS [20].

In order to estimate the performance of the antenna under plasma loading conditions, it was simulated using seawater, which is a simplified plasma mimic material [21–23]. In the simulation for the coupling analysis between the antenna and the plasma, the boundary conditions of −X, ± Y, ± Z planes which are outermost plane of simulation domain are set to PML boundary condition without additional air gaps and on the −X plane, electric field of tangential component is set to zero as shown in Fig. 10.

The dimensions of the sea water (ε_r = 74, σ = 3.53 [s/m]) were 1600 mm, 1000 mm, and 500 mm in the toroidal, poloidal, and radial direction respectively. The surface facing the antenna side was modeled with a curvature similar to that of antenna as shown in Fig. 8. The radial gap between the antenna and sea water was 10 mm. The peak $n_{||}$ and resonant frequency were slightly up-shifted compared with vacuum loading case, and S_{21} was significantly reduced (~13 dB) while maintaining similar S_{11} with vacuum loading as shown in Fig. 11.

Fig. 12 shows the calculated poloidal component of the electric field in front of the antenna for two different coupling cases. The two dotted lines are the envelope lines of the electric field of different coupling conditions. It can be seen that the decay curve of the electric field, along with the toroidal direction changes depending on the coupling. When simulating the decay electric field curve, port (1) was excited 1W input power while port (2) was terminated to a load with 50 Ω. Reducing the radiated power per unit current strap can reduce the up-shift of resonant frequency and peak $n_{||}$ in the plasma loading condition. This means that, in order to minimize the distortions, a sufficient number of current straps in the toroidal direction were required, or that the TWA should be operated under suitable operation conditions with restricted coupling. However, these level of distortions are acceptable value and we expect that the prototype TWA works successfully like mock-up TWA did [8].

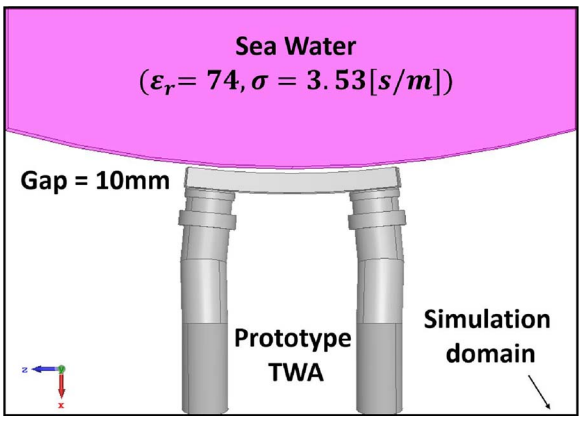

Fig. 10. 3D model of prototype TWA with sea water.

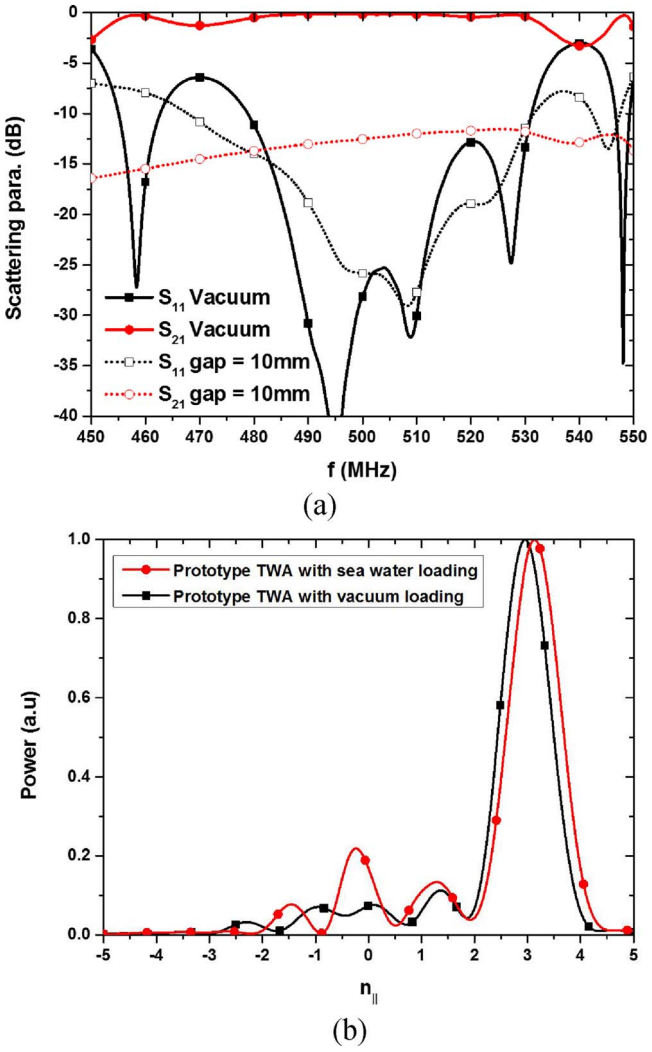

Fig. 11. Simulated results of prototype TWA with vacuum load and sea water loading; (a) scattering parameters, and (b) power spectrum.

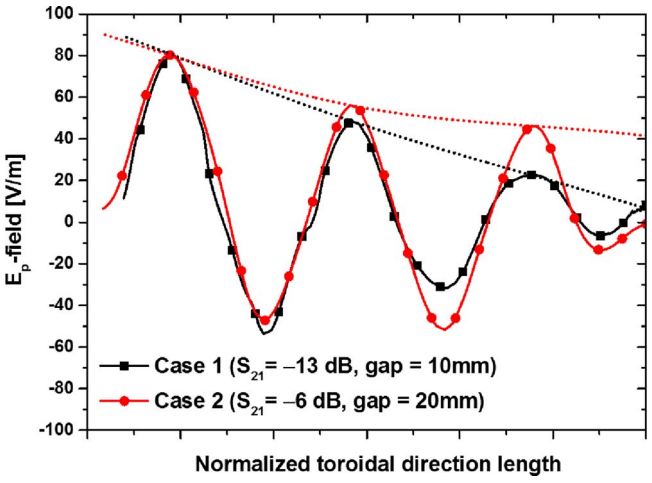

Fig. 12. The simulated electric field in front of the antenna for different coupling.

3. Fabrication and measurement results of prototype TWA

Fig. 13 shows the front and rear views of the fabricated prototype TWA with a back-plate removed. All structure was made of copper. The current straps and antenna ground casing were fabricated to be assembled with screw, and Faraday shield was welded to the antenna ground casing. Fig. 14 shows the photograph of prototype TWA installed in the KSTAR tokamak. The prototype TWA was installed in the same position as the mock-up TWA, approximately 30 cm above the equatorial plane and 0.5 cm behind the poloidal limiters. In order to protect the surface of prototype TWA from plasma heat/particle loads and to reduce copper evaporation into plasma, the front surface of the prototype TWA was coated by tungsten with a thickness of 50 um.

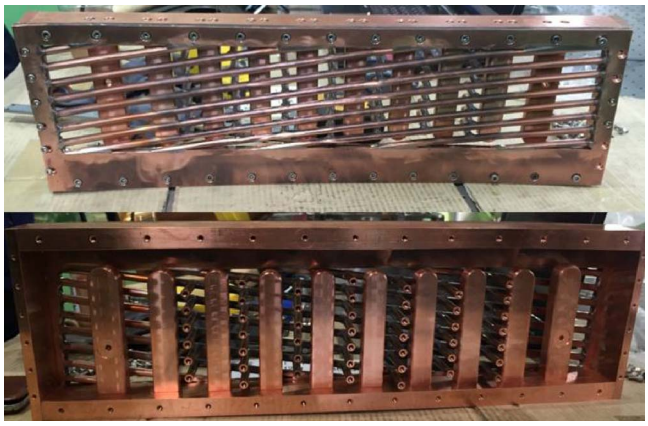

Fig. 13. Photograph of fabricated prototype TWA; front face(up), and rear face (down) with back-plate removed.

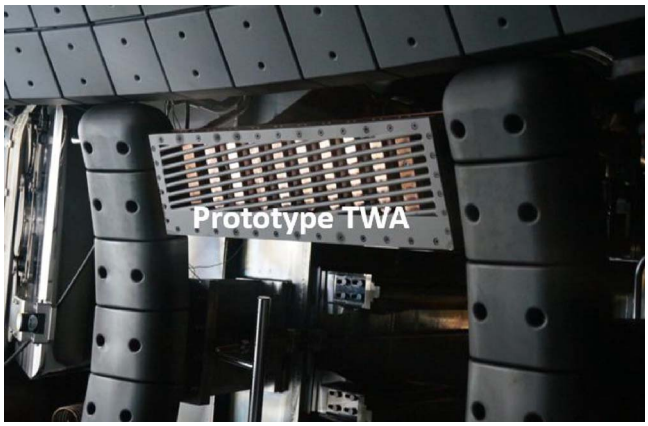

Fig. 14. Photograph of installed prototype TWA in KSTAR.

The RF characteristics of the fabricated prototype TWA were measured using a two port VNA while the prototype TWA was installed in the KSTAR tokamak with RF vacuum windows as shown in Fig. 15. The simulation and measurement results of the prototype TWA were found to be in good agreement, and the $S_{21} = -0.55$ dB at 500 MHz was measured. This was caused by the Ohmic loss at the vacuum transmission line and the dielectric loss at the RF vacuum windows.

4. Summary and conclusion

The proof of principle test of helicon current drive, as a research for a new concept of current drive for reactor-relevant tokamak, has been performed in the KSTAR. The low power coupling test has successfully conducted using a mock-up TWA. In the next step, in order to investigate the high power effects, a prototype TWA based on a mock-up TWA has been designed, fabricated and measured for a medium power RF system. The simulation and measurement results were in good agreement in terms of impedance bandwidth, scattering parameters and $n_{||}$ spectrum, and it is expected that the prototype TWA will work properly with expected performance such as fairly good coupling with the load resiliency, just as mock-up TWA. For actual off-axis current

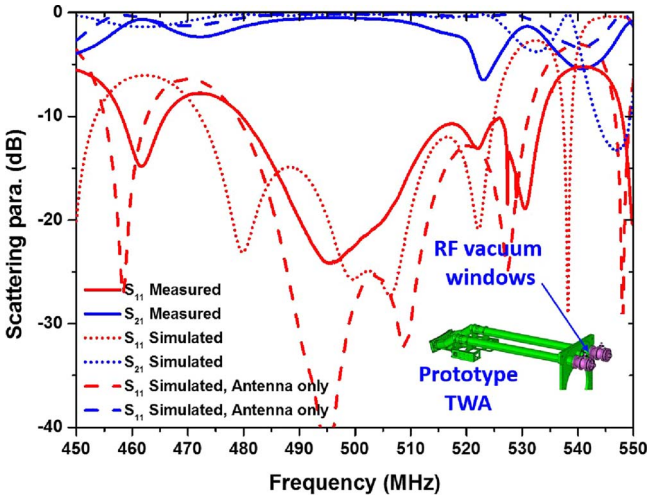

Fig. 15. Simulated and measured scattering parameters of prototype TWA.

drive application, KSTAR is preparing a 1 MW helicon current drive system including development of high power RF components such as a water-cooled antenna and RF vacuum windows.

Acknowledgment

This work was supported by R&D Program through the NFRI funded by the Government funds.

References

[1] R. prater, et al., Non-inductive current drive experiments on DIII-D and future plans, Fusion Eng. Des. 26 (1–4) (1995) 49–58.
[2] R. prater, et al., Application of very high harmonic fast waves for off-axis current drive in the DIII-D and FNSF-AT tokamaks, Nucl. Fusion 54 (2014) 083024.
[3] V.L. Vdovin, Current generation by helicons and lower hybrid waves in modern tokamaks and reactors ITER and DEMO scenarios, modeling and antennae, Plasma Phys. Rep. 39 (2) (2013) 95–119.
[4] R.I. Pinsker, Whistlers, helicons, and lower hybrid waves: the physics of radio frequency wave propagation and absorption for current drive via Landau damping, Phys. Plasmas 22 (2015) 090901.
[5] T. Ogawa, et al., Radiofrequency experiments in JFT-2M: demonstration of innovative applications of a travelling wave antenna, Nucl. Fusion 41 (1767) 2001.
[6] H. Ikezi, et al., Traveling wave antenna for fast-wave heating and current drive in tokamaks, Fusion Technol. 31 (1997).
[7] W.L. Stutzman, G.A. Thiele, Antenna Theory and Design, Wiley, New York, 1998.
[8] S.J. Wang, et al., Helicon wave coupling in KSTAR plasmas for off-axis current drive in high electron pressure plasma, Nucl. Fusion 57 (2017) 046010.
[9] K.K. Kirov, et al., Effects of ICRF induced density modifications on LH wave coupling at JET, Plasma Phys. Control. Fusion 51 (2009) 044003.
[10] M. Porkolab, et al., Parametric instabilities in a magnetic field and possible applications to heating of plasma, Nucl. Fusion 12 (1972) 329.
[11] CST MWS, https://www.cst.com.
[12] R.I. Pinsker, et al., Development of impedance matching technologies for ICRF antenna arrays, Phys. Control. Fusion 40 (1998) A215–A229.
[13] E.M.T. Jones, J.T. Bolljahn, Coupled strip transmission line filters and directional couplers, IRE Trans. Microwave Theory Tech. 4 (1956) 75.
[14] G. T-Penalva, et al., A simple method to design wide-band electronically tunable combline filters, IEEE Trans. Microwave Theory Tech. 50 (1) (2002) 172–177.
[15] I.C. Hunter, et al., Electronically tunable microwave bandpass filters, IEEE Trans. Microwave Theory Tech. 30 (9) (1982) 1354–1360.
[16] J.A. Heikkinen, Electrostatic wave generation by the Faraday shield in ICRF heating, Phys. Lett. A 152 (3–4) (1991).
[17] S.J. Wang, et al., Recent experimental results of KSTAR RF heating and current drive, AIP Conf. Proc. 1689 (2015) 030014.
[18] R. Levy, et al., Transitional combline/evanescent-mode microwave filters, IEEE Trans. Microwave Theory Tech. 45 (12) (1997) 2094–2099.
[19] A.C. England, et al., Power transmission and coupling for radio frequency heating of plasmas, Nucl. Fusion 29 (1527) 1989.
[20] ANSYS HFSS, https://www.ansys.com.
[21] A. Messiaen, et al., Study of ITER ICRH system with external matching by means of a mock-up loaded by a variable water load, Nucl. Fusion 46 (2006) S514.
[22] P.U. Lamalle, et al., Recent developments in ICRF antenna modelling, Nucl. Fusion 46 (2006) 432.
[23] A. Messiaen, et al., Simulation of ICRF antenna plasma loading by a dielectric dummy load application to the ITER case, Fusion Eng. Des. 86 (2001) 855–859.